Engineering Structures 244 (2021) 112765

Contents lists available at ScienceDirect

Engineering Structures

journal homepage: www.elsevier.com/locate/engstruct

Strengthening of shear-deficient RC beams using near surface embedded precast cement-based composite plates (PCBCPs)

Hamdy M. Afefy [a,b,*], Ahmed T. Baraghith [a], Ali Hassan [a], Mohamed K. Abuzaid [b]

[a] Department of Structural Engineering, Faculty of Engineering, Tanta University, Tanta, Egypt
[b] Construction Engineering and Management Department, Faculty of Engineering, Pharos University, Alexandria, Egypt

ARTICLE INFO

Keywords:
Shear-deficient beams
Strain-hardening cementitious composite (SHCC)
Precast cement-based composite plates (PCBCPs)
Crack width
Strengthening

ABSTRACT

Precast cement-based composite plates (PCBCPs) have been prepared, cured and then used to strengthen shear-deficient reinforced concrete (RC) beams. The used PCBCPs have rectangular cross-sections of 100 mm width and 20 mm thickness made of strain-hardening cementitious composite (SHCC) material and reinforced with mild steel plates of 1 mm thickness having variant reinforcement ratios (1.4, 2.8, and 4.2%). The motivation of using such reinforced composite plates is to make use of the mutual benefits between the used materials where the internal steel plate alleviates the cracks localization manifested by plain SHCC material after cracking, while the SHCC material protects the steel plates against corrosion. Experimental test results showed that the use of PCBCPs significantly increased the ultimate shear capacity of the strengthened beams. Besides, inclined configuration of the PCBCPs showed higher shear performance compared to that exhibited by the vertical configuration from both the ultimate capacity and shear cracks characteristics viewpoints. Beam $B_{3\text{-}56\text{-}100\text{-}45}$ strengthened by inclined PCBCPs showed the best performance among all tested beams. It exhibited about 126% increases in the ultimate capacity compared to that of the control un-strengthened beam. On the other hand, the corresponding increase of counterpart beam reinforced with vertical plates was about 88%.

1. Introduction

Commonly, during the service-life of Reinforced Concrete (RC) structures, there is a necessity for strengthening of their members in order to upgrade the ultimate load-carry capacity and/or to satisfy serviceability requirements. In the last decades, external bonding (EB) technique has been widely used for strengthening of RC beams in both flexure and shear. This technique implies the application of thin steel plates to either tensile or shear regions using mechanical anchors or epoxy adhesive.

Various research studies have been conducted in order to assess the efficiency of the EB steel plates technique for shear strengthening of RC beams [1–6]. These studies showed that the EB steel plates could effectively improve the beam's strength, stiffness and ductility [3]. However, the EB steel plates have some issues that may compromise the effectiveness of their applications. These issues include debonding of the steel plates when epoxy adhesive is used, lack of protection such as corrosion and fire and stress concentration produced by the used mechanical anchorage devices used instead of the epoxy adhesive [4]. Near Surface Embedded (NSE) steel plates/rods is another strengthening technique that has been used for the application of externally bonded steel plates. In this technique, using an adequate adhesive material, steel plates/rods are bonded to the sides of the concrete beams through pre-prepared grooves on the concrete cover. Previous work has shown the effectiveness of this method for avoiding the debonding failure of the plates/rods [4,7–9].

Strain-Hardening Cementitious Composite (SHCC) is a class of fiber reinforced cement mortars that exhibits ductile behavior under tensile loading conditions [10]. SHCC is characterized by its strain-hardening response instead of the tension-softening phenomenon demonstrated by the ordinary fiber-reinforced cement composites after first crack initiation [11]. The distinguished strain- hardening phenomenon of the SHCC through micro-cracking is achieved by micromechanical tailoring of its components (binder, fine aggregate, water and fibers) [12–15]. The unique fracture property of the SHCC can be attained through the careful customization and proportioning of its ingredients such as selection of fibers strength and their aspect ratio as well as the interfacial properties of fibers and the matrix [10].

Numerous studies have shown the adequacy of the SHCC material in upgrading and/or restoring the load-carrying capacity of defected RC

* Corresponding author.at: Construction Engineering and Management Dept., Faculty of Engineering, Pharos University, Alexandria, Egypt.
E-mail addresses: hamdy.afefy@pua.edu.eg, hamdy.afefy@f-eng.tanta.edu.eg (H.M. Afefy).

https://doi.org/10.1016/j.engstruct.2021.112765
Received 10 January 2021; Received in revised form 7 June 2021; Accepted 22 June 2021
Available online 30 June 2021
0141-0296/© 2021 Elsevier Ltd. All rights reserved.

members [16–26]. Besides, previous experimental investigations in which SHCC was applied as a surface protection material for both concrete and steel structures demonstrated that the narrow micro cracks of the SHCC provides higher resistance against the penetration of substances such as water, carbon dioxide and oxygen [27]. Accordingly, the application of SHCC coating, changes the corrosion mechanism at the rebar surface from macro cell corrosion to micro cell corrosion [28]. The surface protection performance of the SHCC is associated with both a durable matrix and multiple fine cracks. However, the strain capacity , which is associated with crack distribution, is threatened due to its heterogeneity (e.g. fiber distribution, element size, location of defects in matrix, etc.) [29,30]. In order to sidestep the crack localization and to increase the strain capacity of the SHCC, using of steel reinforcement inside the SHCC was recommended by several researchers. Fischer and Li [31] reported the enhanced tension stiffening behavior of structural elements consists of SHCC and steel reinforcement. Rokugo et al. [32] also revealed the effectiveness of steel reinforcement on the structural response of SHCC/steel composite elements. Kunieda et al. [33] demonstrated the effectiveness of steel reinforcement in enhancing the post-cracking stiffness and post-ultimate deformability of test specimens subjected to tension.

The main target of the current study is to assess the adequacy of precast cement-based composite plates (PCBCPs) for the shear strengthening of RC shear-defected beams. Composite SHCC/steel plates have mutual benefits where the SHCC is able to protect the internal steel plates against corrosion and sidestep the cumbersome application procedure of external steel plates. On the other hand, internal steel plates mitigate the stress localization developed in the SHCC material. For investigation of the shear behavior of RC beams strengthened with the proposed PCBCPs, different governing parameters were studied. Besides, the test results in form of mode of failure, ultimate load, load deflection response and shear crack width measurements are presented, compared and analyzed.

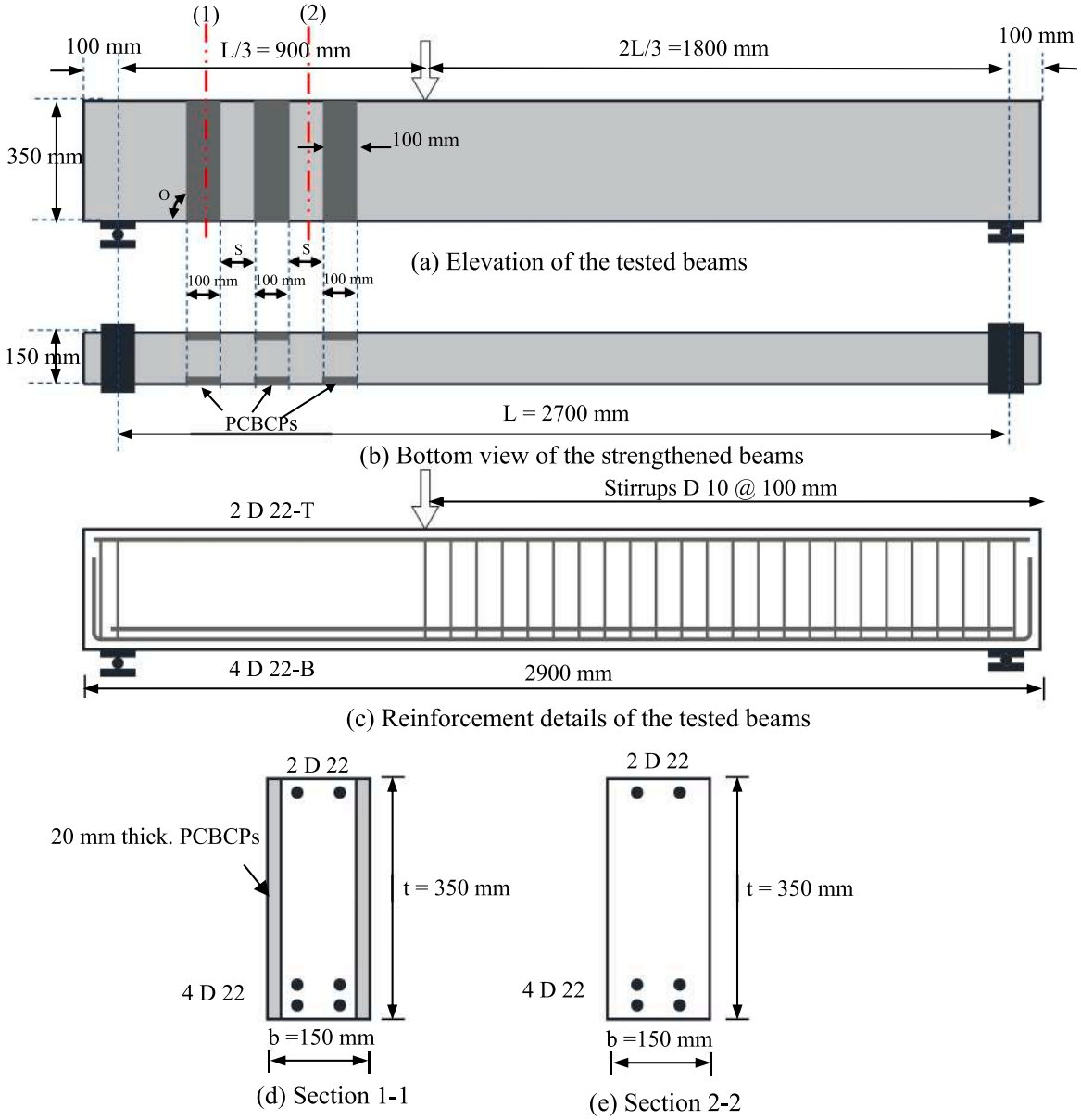


Fig. 1. Details of the tested beams.

2. Experimental work program

2.1. Test beams

The experimental program consisted of twelve typically simply-supported shear-deficient RC beams where one shear span for all beams was intentionally un-reinforced in shear. That is to verify the adequacy of the proposed strengthening system. Fig. 1 shows the concrete dimensions as well as the adopted reinforcement detailing in both longitudinal and transverse directions. All beams had the same length of 2900 mm and cross-sectional dimensions of 150 mm width by 350 mm depth, while the center-to-center span was 2700 mm. For all beams, the thickness of concrete cover of the tensile steel bars was kept constant at 50 mm, yielding an effective depth (d) of 300 mm. All beams were loaded by a single concentrated load at the third point divided the center-to-center span to unequal two shear spans. The long shear span was properly reinforced in shear to avoid the occurrence of shear failure at that shear span where the short shear span was left without vertical stirrups. The short shear span length was 900 mm corresponding to three times of the beam's effective depth, as per ACI 318–19 code [34] recommendation in order to assure a negligible arch action effect. Besides, the flexural reinforcement was chosen in such a way to avoid flexural failure. Thus, all beams were designed and configured to be failed due to shear in the short shear span. The longitudinal reinforcement consisted of four deformed steel bars of 22 mm diameter at the tension side, while the compression reinforcement consisted of two deformed steel bars of 22 mm diameter. The long shear span of the tested beams reinforced with vertical stirrups made of smooth bars having 10 mm diameter and spaced at 100 mm along the entire shear span. On the other hand, only two stirrups having 10 mm diameter were provided at the support zone in order to hang the longitudinal reinforcement.

One beam of the experimental program was control un-strengthened beam, while eleven beams were strengthened in shear using near surface embedded precast cement-based composite plates (PCBCPs) as summarized in Table 1. The used PCBCPs had constant cross-sectional dimensions of 100 mm width and 20 mm thickness. The PCBCPs reinforced with ductile smooth steel plates of 1.0 mm thickness having variable widths. The studied parameters included the width of the steel plate embedded inside the PCBCPs (28, 56 and 84 mm), the clear spacing between the PCBCPs (0, 100, 150 and 200), the number of PCBCPs (3, 4 and 5), and the inclination angle of the installed PCBCPs with respect to the beam's horizontal axis (45°, 60° and 90°).

Table 1
Test matrix.

Group No.	Beam ID	PCBCPs				Objectives
		N	w_s, mm	S, mm	θ, degree	
Control	BC	—	—	—	—	Reference beam
Group I	$B_{3\text{-}0\text{-}100\text{-}90}$	3	—	100	90	Studying the effect of cross-sectional area of internal steel plate inside PCBCPs
	$B_{3\text{-}28\text{-}100\text{-}90}$	3	28	100	90	
	$B_{3\text{-}56\text{-}100\text{-}90}$	3	56	100	90	
	$B_{3\text{-}84\text{-}100\text{-}90}$	3	84	100	90	
Group II	$B_{3\text{-}56\text{-}0\text{-}90}$	3	56	0	90	Studying the effect of PCBCPs clear spacing
	$B_{3\text{-}56\text{-}150\text{-}90}$	3	56	150	90	
	$B_{3\text{-}56\text{-}200\text{-}90}$	3	56	200	90	
Group III	$B_{4\text{-}56\text{-}100\text{-}90}$	4	56	100	90	Studying the effect of PCBCPs number
	$B_{5\text{-}56\text{-}100\text{-}90}$	5	56	100	90	
Group IV	$B_{3\text{-}56\text{-}100\text{-}45}$	3	56	100	45	Studying the effect of PCBCPs inclination angle
	$B_{3\text{-}56\text{-}100\text{-}60}$	3	56	100	60	

PCBCPs = Precast Cement-Based Composite Plates; N = number of PCBCPs; W_s = width of the used steel plate reinforcement; S = clear spacing between the PCBCPs; θ = inclination angle of the PCBCPs with horizontal in degree.

2.2. Beam nomenclature

The beam nomenclature consists of 4 subscript symbols separated by dashes. The first symbol indicates the number of precast plates at each side of the assigned beam at the deficient shear-span zone (3 = three plates, 4 = four plates, 5 = five plates). The second nomenclature stands for the width of the internal steel plate inside the PCBCPs (0 = case of plain plates without internal steel; 28, 56, 84 = the width of internal steel plates are 28, 56 and 84 mm, respectively). The third symbol refers to the typical clear spacing between plates (0 = contiguous plates; 100, 150, 200 = clear spacing between plates are 100, 150 and 200 mm, respectively). The fourth symbol indicates the inclination angle between the plates and the longitudinal axis of beam (90 refers to vertical plates, while 45 and 60 mean that inclined PCBCPs are used where their inclination angles with horizontal axis are 45° and 60°, respectively).

2.3. Material properties

It is well known that the shear strength of RC beams is mainly dependent on the concrete strength. Therefore, a ready-mix concrete patch of target concrete cylinder compressive strength of about 30 MPa was used in order to cast all tested beams at the same time, and then all beams were cured at the same conditions. In addition, standards cylinders of 300 mm height and 150 mm diameter were cast alongside with the beams and cured at the same conditions. That is to assure the consistency of the concrete characteristics in all beams. The ingredients of the used concrete mix for cubic meter are listed in Table 2 as obtained from the supplier of the ready mix. At the testing day, uniaxial compression tests were carried out on nine 150x300 mm concrete cylinders per ASTM C39/C39M [35]. The obtained average compressive strength was about 31.2 MPa. In addition, the splitting tensile tests were carried out on three 150x300 mm concrete cylinders. The obtained average indirect tensile strength of the used concrete was about 3.22 MPa.

Steel reinforcing bars of 22 and 10 mm diameters were used for longitudinal and transversal web reinforcement, respectively. In order to obtain the tensile characteristics of the used steel reinforcing bars, tension tests were performed on three typical specimens for each bar's size. It was found that the longitudinal reinforcing bars (22 mm diameter) had an average yield and ultimate strengths of about 405 and 620 MPa, respectively. Whereas, the transversal reinforcing bars (10 mm diameter) had an average ultimate and yield strengths of about 280 and 425 MPa, respectively.

The strain-hardening cementitous composites (SHCC) material was used as the cementitious matrix to form the proposed strengthening PCBCPs. The ingredients of the SHCC material for cubic meter are listed in Table 2. The used fiber in the SHCC material was polypropylene (PP) fibers and its volume fraction in the mix was about 2.0%. According to the manufacturer's datasheet, the PP fibers had a diameter of 0.025 mm and an average length of 12 mm. The water-to-binder ratio was about 0.20. The binder materials consisted of Silica fume and Ordinary Portland cement 52.5R. Fifteen percent of the design cement content was replaced by silica fume. Fine Quartz sand with diameter less than 0.5 mm was used in the SHCC mix. A high water-reducing admixture was used to enhance the flowability of the matrix.

Standard tensile tests were carried out per ASTM A770/770 M [36] on three standard specimens of the used steel plates for reinforcing the PCBCPs. The average yield and ultimate strengths were about 245 and 360 MPa, respectively. In Addition, the modulus of elasticity was about 202 GPa.

Table 2
Mix proportions of the used materials (kg/m^3) for cubic meter.

W/B	Water	Super plasticizers	Fiber (Volumetric ratio %)	Coarse aggregate	Sand	Silica fume	Cement	Material
0.50	175	—	—	1279	535	—	350	NSC
0.20	312	31.6	16.20 (2.0%)	—	158	237	1342	SHCC

NSC = normal strength concrete; SHCC = Strain-Hardening Cementitious Composites; W/B = water-to-binder ratio

In order to evaluate the effect of using ductile smooth steel plate inside the SHCC material, tensile tests were carried out on both unreinforced and reinforced SHCC specimens. Six typical tensile test specimens had cross-sectional dimensions of 50 × 200 mm and 900 mm length were used where three of them were unreinforced and the remaining three specimens were provided with internal steel plates of 1 mm thickness and 140 mm width. Fig. 2 shows concrete dimensions and reinforcement detailing of typical test specimen along with the provided sensors. Samples of the uniaxial tensile response for reinforced and unreinforced test specimens are depicted in Fig. 3. It can be observed that the reinforced and unreinforced SHCC specimens had almost a similar first cracking strength of about 3.2 MPa. On the other hand, the ultimate tensile strength of reinforced SHCC specimen was about 1.5 times that the corresponding strength of unreinforced specimen due to the contribution of the internal steel plate. The ultimate tensile strengths of unreinforced and reinforced specimens were about 7.05 MPa and 10.46 MPa, respectively. The ultimate tensile strains corresponding to the maximum tensile strengths for unreinforced and reinforced SHCC specimens were about 5050 and 8800 με, respectively. In order to obtain the uniaxial compressive response of the SHCC material, three 50 × 100 mm cylinders were tested. The average compressive cylinder strength of the used SHCC material at the testing day was about 65.5 MPa. Fig. 4 shows a sample of the obtained uniaxial compressive stress–strain response for both SHCC material and plain concrete cylinders. It can be noticed the softening response of the SHCC material compared to the plain concrete material.

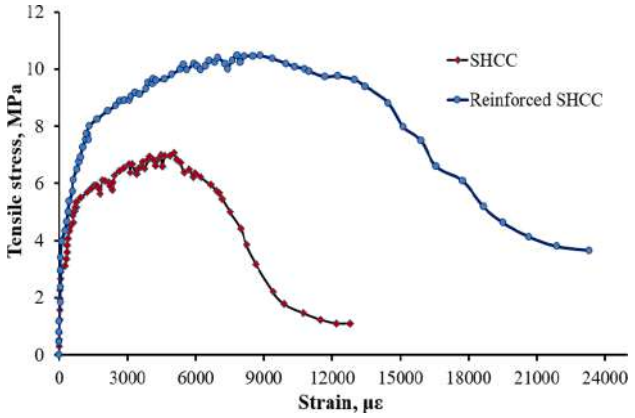
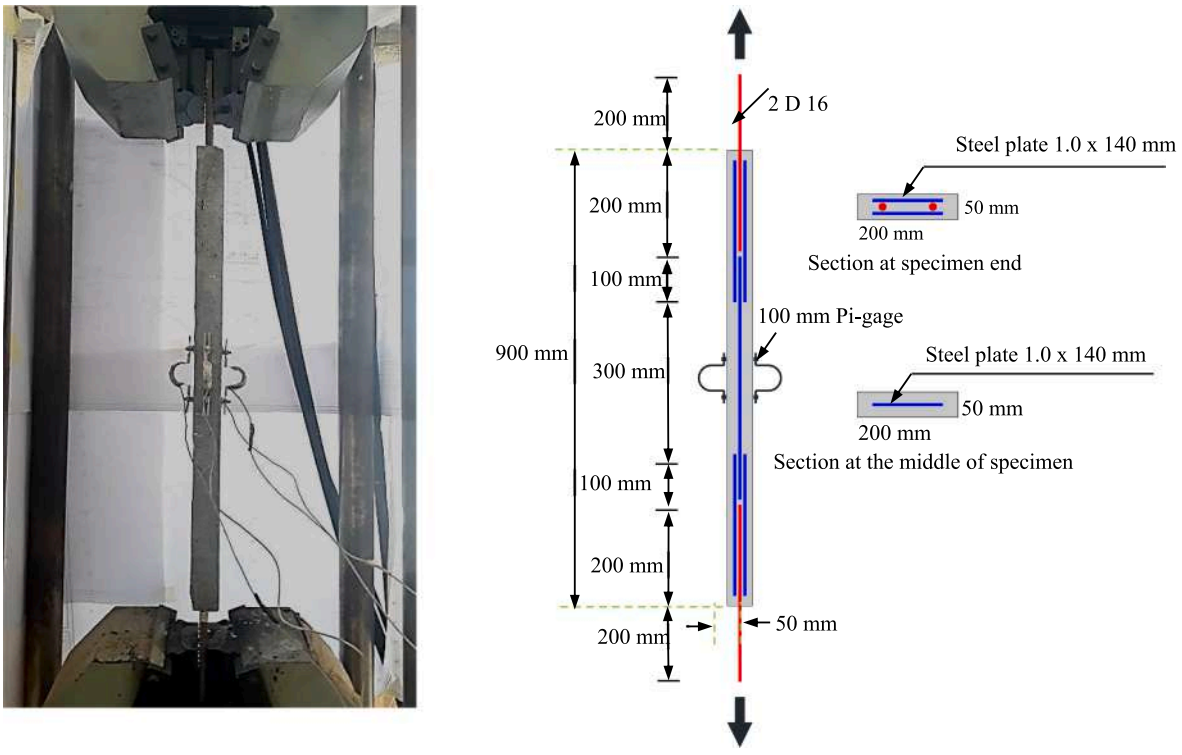


Fig. 3. Samples of stress-strain relationship for SHCC specimens under uniaxial tension.

2.4. Fabrication of the PCBCPs

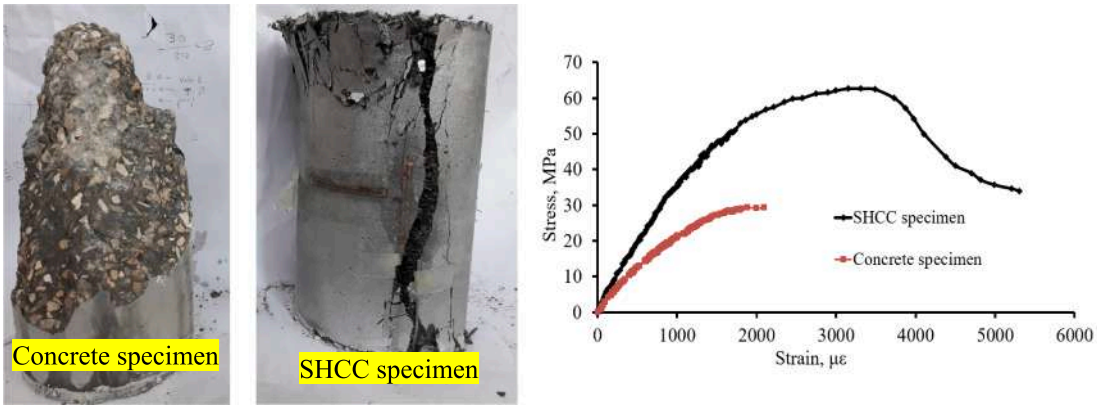
The PCBCPs used in this research composed of prismatic SHCC plates having rectangular cross-section of 20 × 100 mm that were either unreinforced or reinforced with thin steel plates of 1.0 mm thickness as depicted in Fig. 5(a). It can be observed that end hooks were developed



(a) Image of uniaxial tension test setup

(b) Details of the direct tension test specimens

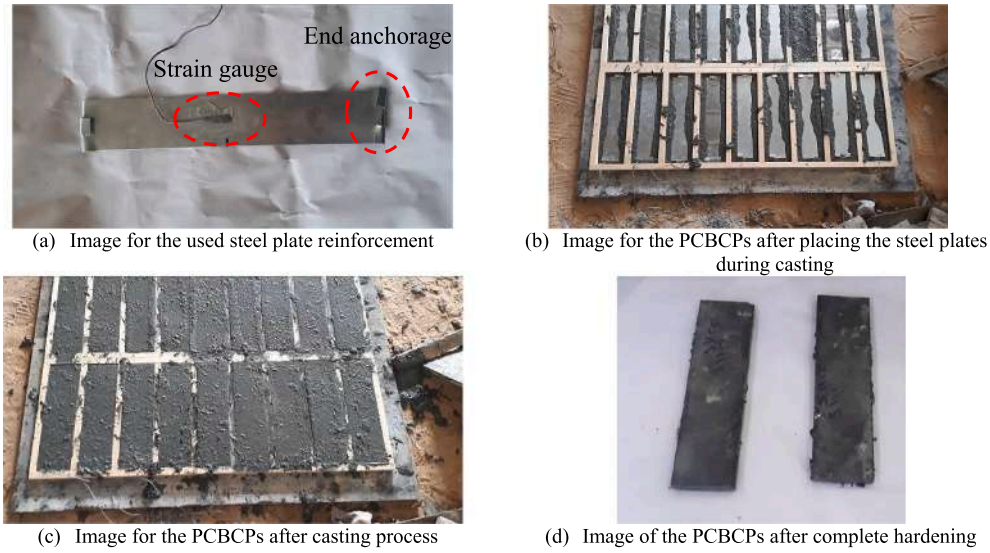
Fig. 2. Uniaxial direct tension test of SHCC specimens.



(a) Samples of the tested cylinders after uniaxial compression test

(b) Samples of stress strain curves for SHCC and concrete under uniaxial compression test

Fig. 4. Uniaxial compression test for concrete and SHCC.



(a) Image for the used steel plate reinforcement

(b) Image for the PCBCPs after placing the steel plates during casting

(c) Image for the PCBCPs after casting process

(d) Image of the PCBCPs after complete hardening

Fig. 5. Fabrication of the PCBCPs.

at both ends of the steel plates in order to increase the bond strength between the SHCC material and the internal steel plate. The width of the internal steel plate was divided into three parts where the outer parts were bent in the opposite side of the middle one. The length of the hook was about 20 mm (20 times the plate thickness). The PCBCPs were cast in horizontal wooden formworks having the required dimensions. For the PCBCPs provided with steel plates, the SHCC material was cast into the wooden molds up to 10 mm thickness (their halves), then the steel plate was placed at the middle thickness of the PCBCPs as depicted in Fig. 5(b). After that, the remaining 10 mm thickness of the SHCC material was cast into the mold to have a total thickness of 20 mm for the PCBCPs as depicted in Fig. 5(c). It is worth mentioning that the upper surfaces of the PCBCPs were left unleveled. That is to have rough surface, which enables good contact with the epoxy adhesive during bonding of the PCBCPs to the substrate beam. Owing to the flowable characteristics of the SHCC material, casting was started from one edge of the formwork and was allowed to flow to the other edge. In order to obtain a similar fiber distribution in all plates, the same casting procedure was used for all plates. Besides, in order to exclude the early-age high shrinkage phenomenon of the SHCC material, the PCBCPs were demolded after 24 h then cured under wet conditions for 14 days, and then allowed air drying as shown in Fig. 5(d).

2.5. *Strengthening application*

Before the application of the PCBCPs to the lateral faces of the defected shear span zones, they were pre-cured for about two months in order to alleviate the volumetric change issues. And then they were applied as follows. First, according to the pre-assigned positions of the PCBCPs, slots of 20 mm depth and 100 mm width were initially grooved in the concrete cover of the beams as depicted in Fig. 6(a). Second, the grooves were grinded to additional 2 mm thickness in each side and cleaned using compressed air in order to keep their surfaces dry and clean as depicted in Fig. 6(b). Third, a high-strength epoxy adhesive material (MasterBrace ADH 2200) of 1 mm thickness was applied to the contact surfaces between the PCBCPs and the substrate surfaces of the concrete beam as depicted in Fig. 6(c). Fourth, another 1 mm epoxy adhesive was applied to the surface of PCBCPs and then placed in their grooves and firmly pressed to reduce any possibility of forming air voids between the PCBCPs and the substrate beam. Finally, mechanical steel clamps were used to hold the PCBCPs in their positions with the lateral faces of the strengthened beam. After about 7 days, the epoxy resin has hardened and reached its full tensile strength. Thus, the strengthened beam using PCBCPs was ready for testing as depicted in Fig. 6(d). It is worth mentioning that the application of the PCBCPs was performed in two consecutive days. Besides, testing of all strengthened beams was



(a) Image of a test specimen after preparing the required grooves

(b) Image during cleaning the grooves

(c) Image of a test specimen during the application of the epoxy adhesive

(d) Image of a test specimen after complete placement of the PCBCPs

Fig. 6. Steps of the application of strengthening PCBCPs.

conducted in another three continuous days. That is to limit any variations in the ultimate strengths for concrete, SHCC material and the epoxy resin.

2.6. Test setup and instrumentation

All beams have been tested under three-point bending test as depicted in Fig. 7. An incremental monotonic load was applied using a load-controlled scheme with an average loading rate of about 10 kN/min till failure where the acting load was measured using a load cell of 500 kN capacity. To trace the developed vertical deflection, three Linear Variable Differential Transformers (LVDTs) were placed under the test specimen to measure the vertical deflections at the mid-span section, the loading point and the middle of the strengthened shear span. Besides, two LVDTs were placed over both supports in order to record any possible support movement during the test. In order to measure the developed shear strains, another two 45-degree rosette LVDTs were placed on the beam surface at the center of the strengthened shear span. In addition, two electrical strain gauges having 5 mm gauge length were bonded to the tensile and compressive reinforcing bars at the load location in order to measure the developed normal strain in the longitudinal steel bars. Furthermore, for each reinforced PCBCP, a strain gauge was mounted at the middle of the embedded steel plate as depicted in Fig. 5(a). To measure the major crack width, an optical microscope of 0.01 mm accuracy was used. For each test, an automatic data acquisition unit was used to record and store data during testing for the load cell, LVDTs, and the strain gauges.

3. Experimental results

3.1. Mode of failure

Fig. 8 shows the exhibited modes of failure for the control unstrengthened and strengthened beams just before complete failure. It can be observed that all strengthened beams as well as the control unstrengthened beam developed shear failure mode, as configured, owing to the propagation of shear cracks within the critical shear span zone. For all strengthened beams using vertical PCBCPs, except $B_{3\text{-}56\text{-}0\text{-}}$

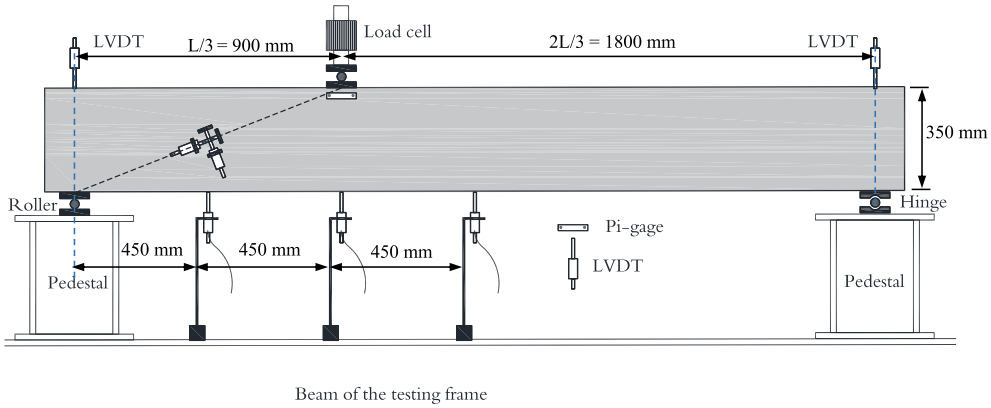


Fig. 7. Test setup and instrumentation.

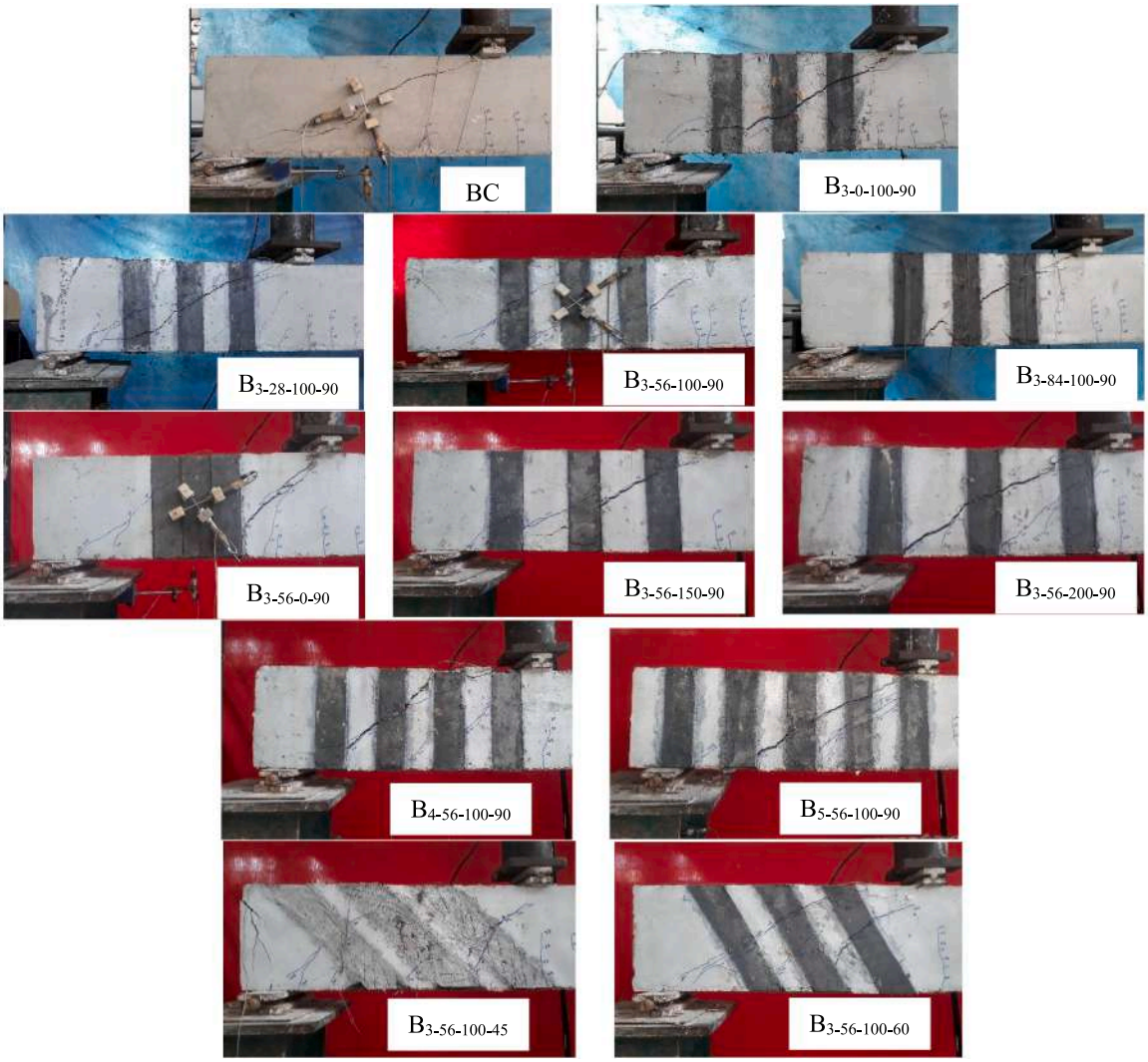


Fig. 8. Failure modes of un-strengthened and strengthened beams.

$_{90}$, the failure was characterized by the formation of a major diagonal shear crack intersecting the PCBCPs in the direction of the line connecting the loading and support points. In addition to the major shear crack, additional diagonal cracks were formed and distributed along the critical shear span zone. It is worth mentioning that, the failure was governed by PCBCPs rupture without any signs of PCBCPs/concrete debonding or delamination. As for beam $B_{3\text{-}56\text{-}0\text{-}90}$, the contiguous PCBCPs resulted in increased the shear stiffness of the middle zone of the strengthened shear span that triggered shear cracking to take place at the weakest parts in the critical shear span. Therefore, the failure of $B_{3\text{-}56\text{-}0\text{-}90}$ was characterized by the formation of two parallel diagonal shear cracks in the un-strengthened zones in both sides of the strengthened part as shown in Fig. 8, Thus, one crack extended from the loading point to the lower-right part of the contiguous PCBCPs, while the second crack extended from the support point to the upper-left part of the contiguous PCBCPs.

Using inclined PCBCPs resulted in decrease the exhibited shear cracks widths near failure as well as triggered more than one major shear crack to be developed as depicted in Fig. 8. That is because the developed shear cracks were approximately perpendicular to the axes of PCBCPs. Consequently, the corresponding failure loads were higher than the opponent load of the strengthened beam using vertical PCBCPs as presented in Table 3.

3.2. Ultimate loads

Table 3 summarizes the experimental test results including the ultimate shear capacity (P_u), strength gain due to the application of PCBCPs, vertical deflection under the loading point corresponding to the ultimate load (δ_u), and the absorbed energy (E).

Generally, as summarized in Table 3, the use of PCBCPs significantly increased the ultimate capacity (P_u) of the strengthened beams, which demonstrates a powerful implementation of the proposed strengthening technique for RC shear deficient beams. Compared to the un-strengthened beam, the use of unreinforced PCBCPs made of SHCC material only enabled the beam $B_{3\text{-}0\text{-}100\text{-}90}$ to increase its ultimate capacity by about 29% compared to that of the un-strengthened beam. Moreover, as expected, using thin steel plates to reinforce the SHCC plates resulted in increased the axial stiffness and strength of the used PCBCPs, thus, enhanced the shear capacity of the strengthened beams. Fig. 9 shows the relationship between the plate reinforcement ratio and the percentage of enhancement in the ultimate shear capacity for all beams of group I. It can be observed that the gain in the ultimate capacity is directly proportionate to the plate reinforcement ratio. Thus, the highest gain in the ultimate capacity was recorded for beam $B_{3\text{-}84\text{-}100\text{-}90}$ that reached up to about 115% corresponding to the highest reinforcement ratio of 4.25%, compared to that of the un-strengthened control beam BC.

Beams $B_{3\text{-}56\text{-}0\text{-}90}$, $B_{3\text{-}56\text{-}100\text{-}90}$, $B_{3\text{-}56\text{-}150\text{-}90}$, and $B_{3\text{-}56\text{-}200\text{-}90}$ have been

Table 3
Test results.

Group No.	Beam ID	P_u, kN	Strength gain, kN	Δ_u, mm	$\Delta_{0.8u}$, mm	D	E, kN. mm
Control	BC	85.00	—	4.40	4.40	1.00	185
Group I	$B_{3\text{-}0\text{-}100\text{-}90}$	109.82	24.82	5.34	6.15	1.15	309
	$B_{3\text{-}28\text{-}100\text{-}90}$	136.40	51.40	7.66	9.10	1.19	545
	$B_{3\text{-}56\text{-}100\text{-}90}$	160.50	75.50	9.52	11.57	1.22	845
	$B_{3\text{-}84\text{-}100\text{-}90}$	183.02	98.02	12.40	15.50	1.25	1385
Group II	$B_{3\text{-}56\text{-}0\text{-}90}$	134.98	49.98	7.84	7.84	1.00	584
	$B_{3\text{-}56\text{-}150\text{-}90}$	143.80	58.80	8.44	9.17	1.09	717
	$B_{3\text{-}56\text{-}200\text{-}90}$	126.14	41.14	7.50	8.05	1.08	527
Group III	$B_{4\text{-}56\text{-}100\text{-}90}$	172.60	87.60	9.47	11.64	1.23	860
	$B_{5\text{-}56\text{-}100\text{-}90}$	169.20	84.20	9.49	11.62	1.22	852
Group IV	$B_{3\text{-}56\text{-}100\text{-}45}$	192.22	107.22	10.16	12.87	1.27	943
	$B_{3\text{-}56\text{-}100\text{-}60}$	175.17	90.17	9.66	11.95	1.24	890

P_u = ultimate load; Δ_u = deflection corresponding to ultimate load; $\Delta_{0.8u}$ = deflection at a descending load corresponding to 0.8 of ultimate load; D = displacement-based ductility index ($D = \Delta_{0.8u}/\Delta_u$) [39,40]; E = absorbed energy.

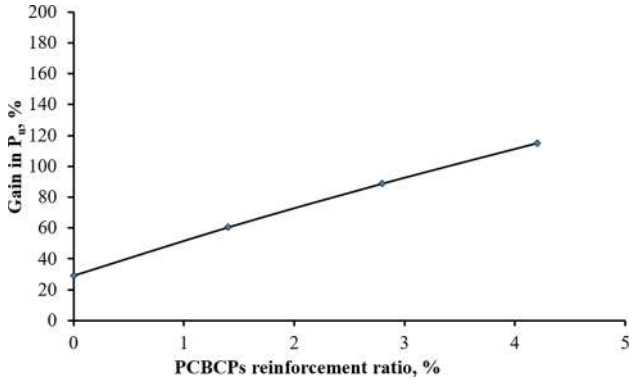


Fig. 9. Gain in ultimate sustained load versus PCBCPs reinforcement ratio.

strengthened with PCBCPs having the same reinforcement ratio, where the clear spacing between the plates was varied. The experimental results showed that the use of distributed PCBCPs showed better enhancement in the load-carrying capacity for the strengthened beams $B_{3\text{-}56\text{-}100\text{-}90}$, $B_{3\text{-}56\text{-}150\text{-}90}$, and $B_{3\text{-}56\text{-}200\text{-}90}$ than that developed by beam $B_{3\text{-}56\text{-}0\text{-}90}$ having contiguous PCBCPs (clear spacing = 0 mm). This could be attributed to that using contiguous PCBCPs, keeping 300 mm in both ends of the critical shear span without any strengthening plates, forced the failure to be occurred in the un-strengthened length in both sides of the strengthened part. Thus, the ultimate capacity of beam $B_{3\text{-}56\text{-}0\text{-}90}$ was lower than the corresponding capacity of beam $B_{3\text{-}56\text{-}100\text{-}90}$ by about 16%. Increasing the clear spacing between the PCBCPs decreased the ultimate capacity of the beams $B_{3\text{-}56\text{-}150\text{-}90}$, and $B_{3\text{-}56\text{-}200\text{-}90}$ by about 10% and 21% compared to that developed by beam $B_{3\text{-}56\text{-}100\text{-}90}$. This is a fact as increasing the spacing between the PCBCPs decreases the added reinforcement ratio, thus decreased the efficiency of the strengthened beam.

Group III consists of two beams $B_{4\text{-}56\text{-}100\text{-}90}$ and $B_{5\text{-}56\text{-}100\text{-}90}$, which were strengthened using 4 and 5 PCBCPs, respectively. The used plates were distributed along the shear span at 100 mm clear spacing. In addition, these plates were positioned to be concentric with the shear span. The experimental results showed that, however the number of the plates was increased from 4 to 5, the ultimate capacity was almost constant. The recorded capacities were 172.60 and 169.2 kN for beams $B_{4\text{-}56\text{-}100\text{-}90}$ and $B_{5\text{-}56\text{-}100\text{-}90}$, respectively. This may be attributed to that when five plates were used in $B_{5\text{-}56\text{-}100\text{-}90}$, the first plate was set over the support point while the last one was set under the loading point, as shown in Fig. 8, which decreases their contributions where the first and the last plates did not interrupt the loading path. It is worth mentioning that the ultimate capacity of beam $B_{3\text{-}56\text{-}100\text{-}90}$ provided with only three plates was about 160.5 kN, which is comparable to the beam provided with five plates.

Group IV was designed to examine the effect of using inclined PCBCPs. Beams $B_{3\text{-}56\text{-}100\text{-}45}$ and $B_{3\text{-}56\text{-}100\text{-}60}$ having two different inclination angles; namely, 45° and 60°, respectively, were tested and their results were compared with those exhibited by beam $B_{3\text{-}56\text{-}100\text{-}90}$ having vertical PCBCPs. The test results indicated that the inclined plates enhanced the shear capacity of the tested beams significantly. The shear capacities of $B_{3\text{-}56\text{-}100\text{-}45}$ (192.22 kN) and $B_{3\text{-}56\text{-}100\text{-}60}$ (175.17kN) were 20% and 9% higher than that of $B_{3\text{-}56\text{-}100\text{-}90}$ (160.50 kN) having vertical plates, respectively. Thus, based on the adopted dimensions, using inclined PCBCPs has better effect than that provided by vertical PCBCPs, especially when the plates were positioned to be perpendicular to the line connecting the load and reaction points.

3.3. Experimental shear capacity versus analytical estimation

Based on the adopted unsymmetrical loading configuration, the maximum shearing force for all beams was developed at the strengthened shear span zone. Thus, the experimental shearing forces were calculated for all strengthened beams as well as the control unstrengthened beam as summarized in Table 4. For the control unstrengthened beam BC, the analytical shear force, $Q_{c(uncrcaked)}$, was calculated per the Egyptian Code of Practice ECP 203–2018 [37] as given by Eq. (1), where the shear force is that corresponding to the initiation of shear cracking.

$$Q_{c(uncrcaked)} = 0.16\sqrt{\frac{f_{cu}}{\gamma_c}}.bd \tag{1}$$

Where f_{cu} = the concrete compressive cube strength (31.2 MPa); γ_c = the strength reduction factor taken as unity for comparison purpose; b = the width of concrete section (150 mm); d = the effective depth (285 mm). As for the strengthened beams, the shear resistance of the composite plates was calculated based on the proposed equation by [38], which was developed to estimate the shear resistance of RC strengthened beams using composite plates neglecting the concrete tensile resistance. Consequently, the ultimate shear capacity of reinforced concrete beams exclusive the contribution of shear resistance for cracked concrete can be calculated by Eq. (2) [38].

$$V_{st} = \frac{A_v f_v d_v}{s.tan\theta} + \frac{A_m f_m d_m}{s_m}\left(\frac{1}{tan\theta} + \frac{1}{tan\alpha}\right) sin\alpha \tag{2}$$

Where $A_v f_v$ = the tensile force resisted by one row of vertical composite plates, which equals to the cross-sectional area of two vertical composite plates (one at each side) multiplied by their tensile resistance; d_v = effective depth of the beam's cross-section; s = spacing between the centerlines of vertical plates; θ = inclination angle of the major shear crack assumed as 45°; $A_m f_m$ = the tensile force resisted by one row of inclined plates; d_m = vertical projection of the plate ; α = inclination angle of the inclined plate with horizontal; s_m = horizontal spacing between the inclined plates ($s_m = \frac{s}{sin\alpha}$). The tensile resistance of composite plates at one row was calculated by Eq. (3).

$$A_v f_v = A_m f_m = 2 f_{tp} b_p t_p + 2 f_{ys} b_s t_s \tag{3}$$

Where f_{tp} is the maximum tensile strength of the SHCC material

Table 4
Analytical shear resistances versus experimental results.

Group No.	Beam ID	P_u, kN	Q_u Exp, kN	Q_{cu}, kN	Q_{PCBCPs}, kN	Q Ana, kN	Q_u Exp/ Q Ana
Control	BC	70.00*	46.67	38.21**	0	38.21	1.22
Group I	$B_{3\text{-}0\text{-}100\text{-}90}$	109.82	73.21	28.65***	17.10	45.75	1.60
	$B_{3\text{-}28\text{-}100\text{-}90}$	136.40	90.93	28.65***	36.65	65.30	1.39
	$B_{3\text{-}56\text{-}100\text{-}90}$	160.50	107.00	28.65***	56.20	84.85	1.26
	$B_{3\text{-}84\text{-}100\text{-}90}$	183.02	122.01	28.65***	75.75	104.40	1.17
Group II	$B_{3\text{-}56\text{-}0\text{-}90}$	134.98	89.99	28.65***	37.47	66.12	1.36
	$B_{3\text{-}56\text{-}150\text{-}90}$	143.80	95.87	28.65***	44.96	73.61	1.30
	$B_{3\text{-}56\text{-}200\text{-}90}$	126.14	84.09	28.65***	37.47	66.12	1.27
Group III	$B_{4\text{-}56\text{-}100\text{-}90}$	172.60	115.07	28.65***	56.20	84.85	1.36
	$B_{5\text{-}56\text{-}100\text{-}90}$	169.20	112.80	28.65***	56.20	84.85	1.33
Group IV	$B_{3\text{-}56\text{-}100\text{-}45}$	192.22	128.15	28.65***	79.48	108.13	1.19
	$B_{3\text{-}56\text{-}100\text{-}60}$	175.17	116.78	28.65***	76.77	105.42	1.11

P_u = total ultimate load; Q_u Exp = experimental ultimate shear force = *0.67* P_u; Q_{cu} = concrete resistance; Q_{PCBCPs} = shear resistance of precast cement-based composite plates; Q Ana = analytical shear force;
* the considered ultimate load is that corresponding to the first shear cracking load;
** uncracking concrete shear resistance;
*** cracked concrete shear resistance

before cracking (3 MPa), b_p is the width of the composite plate (100 mm),t_p is the thickness of composite plate (20 mm), f_{ys} is the yield stress of internal steel plate (245 MPa), b_s is the width of the internal steel plate (28, 56, 84 mm), t_s is the thickness of steel plate (1 mm).

For all strengthened beams, the total analytical shear resistance was calculated as the summation of the shear resistance of the composite plates according to Eq. (2) and the contribution of cracked concrete per the ECP 203–2018 [37] as given by Eq. (4).

$$Q_{c(crcaked)} = 0.12\sqrt{\frac{f_{cu}}{\gamma_c}}.bd \tag{4}$$

Table 4 summarizes the results of both experimental tests and the analytical estimations for all beams. It can be observed that the analytical shear resistance based on the adopted model showed conservative results compared to the experimental findings for all strengthened beams using precast cement-based composite plates. The safety margin ranged from 11% up to 39%.

Obviously, the adopted equation [38] was developed for composite plates; however, it was used to calculate the shear resistance of RC beam strengthened by plain SHCC plates in order to obtain only the contribution of such plates without the internal steel plates. Thus, the difference between the experimental and the analytical resistances of beam $B_{3\text{-}0\text{-}100\text{-}90}$ was about 60%, which confirms that plain SHCC precast plates cannot be used exclusively to strengthen RC beam. On the other hand, reinforced composite plates enabled the strengthened beams to show acceptable differences in the shear resistances, which is about 27% based on average resistances for all strengthened beams. Besides, all calculated shear resistances are in the conservative side where the experimental resistances are higher than the corresponding calculated ones.

It is worth mentioning that the contribution of contiguous composite plates of beam $B_{3\text{-}56\text{-}0\text{-}90}$ was calculated based on one row of PCBCPs having cross-sectional area of 20 mm thickness by 300 mm width corresponding to the summation of the three contiguous plates and centered in one spacing of 900 mm length.

3.4. Load deflection response

Figs. 10 to 13 show the load–deflection relationships for all tested beams. The load deflection response of the un-strengthened beam, BC, was included for the purpose of comparison. For beam BC when the total vertical load reached about 85 kN, the beam failed suddenly and the load dropped sharply from the peak to the release load. Whereas, as shown in Fig. 10, the strengthened beams of group I showed different post-peak behavior in comparison with that exhibited by beam BC. The

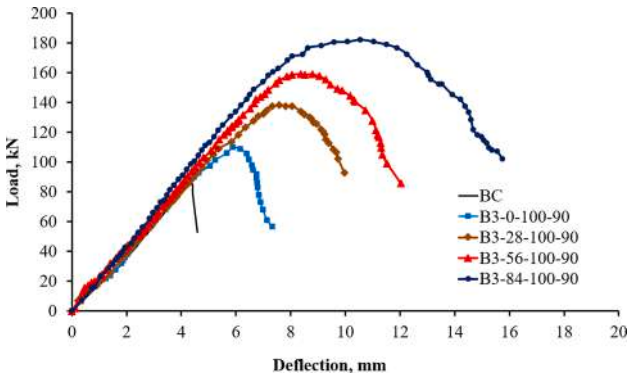


Fig. 10. Load-deflection curves for all beams of group I.

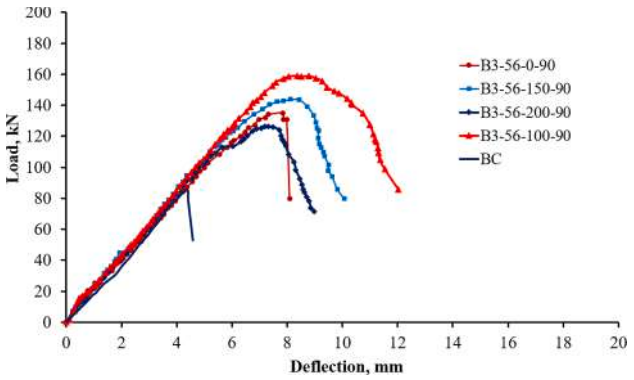


Fig. 11. Load-deflection curves for all beams of group II.

strengthened beams demonstrated softening behaviors during the post-peak stage which represent the shear contributions of the used PCBCPs. Moreover, beams $B_{3\text{-}28\text{-}100\text{-}90}$, $B_{3\text{-}56\text{-}100\text{-}90}$ and $B_{3\text{-}84\text{-}100\text{-}90}$ strengthened with reinforced PCBCPs plates generally exhibited a softer post-peak response compared to that obtained by the counterpart beam $B_{3\text{-}0\text{-}100\text{-}90}$ provided with plain PCBCPs. That could be attributed to the contribution of the internal steel plates.

Group II was designed to study the effect of PCBCPs spacing. In addition to beam $B_{3\text{-}56\text{-}100\text{-}90}$, with plate's spacing of 100 mm, other three clear spacing were studied. Beams $B_{3\text{-}56\text{-}150\text{-}90}$ (clear spacing = 150 mm) and $B_{3\text{-}56\text{-}200\text{-}90}$ (clear spacing = 200 mm) showed load–deflection responses quite similar to that showed by beam $B_{3\text{-}56\text{-}100\text{-}90}$ except that

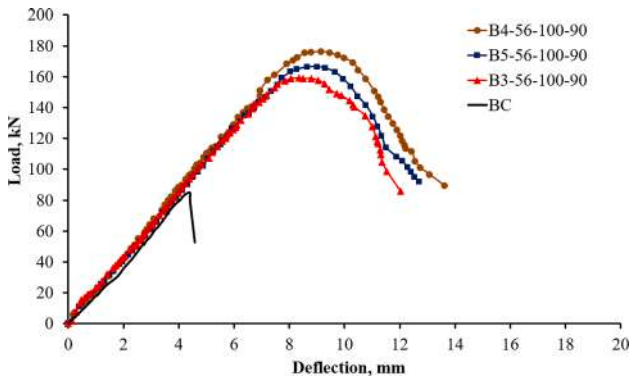


Fig. 12. Load-deflection curves for all beams of group III.

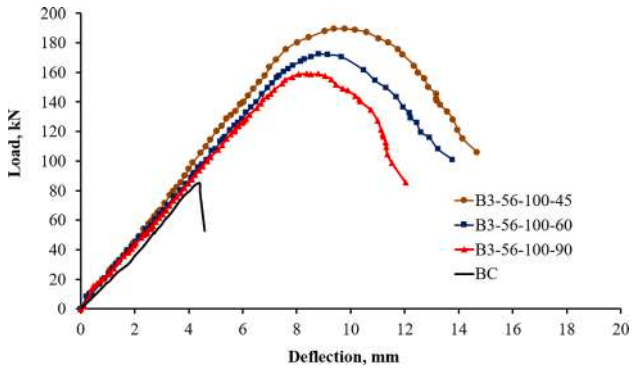


Fig. 13. Load-deflection curves for all beams of group IV.

the ultimate capacity and the corresponding softening plateau were differed based on the value of the clear spacing. Whereas, beam $B_{3\text{-}56\text{-}0\text{-}90}$ provided with contiguous plates exhibited a sudden failure after reaching its ultimate capacity, as depicted in Fig. 11. As previously explained, the shear failure for beam $B_{3\text{-}56\text{-}0\text{-}90}$ took-place in the un-strengthened length of the critical shear span, which is similar to that exhibited by the un-strengthened beam BC. This observation explains the reason for such unexpected obtained response for beam $B_{3\text{-}56\text{-}0\text{-}90}$.

It is worth mentioning that, as shown in Figs. 12 and 13, the increase of plate's number and plate's inclination angle did not alter the undergoing phases of the load–deflection response of groups III and IV.

Columns 5 and 6 of Table 3 report the deflection measurements at ultimate load (Δ_u) and at a descending load level corresponding to 0.80 of the ultimate load ($\Delta_{0.8u}$). Column 7 of Table 3 lists the values of displacement-based ductility index (D) which is defined as the ratio between $\Delta_{0.8u} / \Delta_u$ which may be considered as a measure of ductility for the strengthened specimens [39,40].

Comparing the values of displacement-based ductility index, D, of group I, the strengthened PCBCPs resulted in higher values of D compared with that exhibited by plain PCBCPs. As listed in Table 3, the increases ranged between 15% and 25% compared to that of the reference un-strengthened beam BC, which reflects the ability of the proposed PCBCPs technique in improving the post-peak response of the strengthened beams. In addition, beam $B_{3\text{-}84\text{-}100\text{-}90}$ showed the height value of D ($D = 1.22$), which highlights the effect of plate's internal reinforcement.

For group II, the effect of the plate's spacing on the ductility index D was

significant. Beam $B_{3\text{-}56\text{-}0\text{-}90}$ provided with contiguous plates showed the lowest value of D ($D = 1.0$). The loss in the ductility was probably because of the sudden brittle failure mode of $B_{3\text{-}56\text{-}0\text{-}90}$ that took-place in the un-strengthened length of the critical shear span. Besides, increasing the clear spacing between the PCBCPs from 100 mm to 200 mm resulted in decreased of D by about11%.

For group III, the effect of plate's number on ductility index D was insignificant. Beams $B_{3\text{-}56\text{-}100\text{-}90}$, $B_{4\text{-}56\text{-}100\text{-}90}$ and $B_{5\text{-}56\text{-}100\text{-}90}$, those were strengthened by 3, 4 and 5 PCBCPs, respectively, showed identical D value (i.e.; 1.23 for beam $B_{4\text{-}56\text{-}100\text{-}90}$ vs. 1.22 for beams $B_{3\text{-}56\text{-}100\text{-}90}$ and $B_{5\text{-}56\text{-}100\text{-}90}$ as listed in Table 3).

As for the beams of group IV, strengthened with inclined PCBCPs, the test results showed that the inclination angle has insignificant effect on the ductility index where the ductility indices for beams $B_{3\text{-}56\text{-}100\text{-}45}$ and $B_{3\text{-}56\text{-}100\text{-}60}$ were about 1.27 and 1.24, respectively, corresponding to about 4% and 2% increases compared to that exhibited by the beam provided with vertical plates $B_{3\text{-}56\text{-}100\text{-}90}$.

3.5. Absorbed energy

The absorbed energy (E) is defined as, the integration of the load–deflection curve (the area under the curve) up to the peak load. Column 8 of Table 3 reports the value of E for all beams. As shown in Table 3, the control un-strengthened beam BC recorded the lowest value of E (185 kN.mm). Whereas, all beams provided with PCBCPs at the shear span zone showed higher enhancement in the absorbed energy. Also, it can be noted that, there is a direct relation between plate's internal reinforcement and the values of E. This may be explained by; the addition of steel reinforcement into the PCBCPs not only increased the ultimate load but also increased the ultimate deflection. Thus, beam $B_{3\text{-}84\text{-}100\text{-}90}$ recorded the maximum value of E (1385 kN.mm), which is about 7.48 times that obtained by the reference beam BC (185 kN.mm) and 4.48 times that obtained by beam $B_{3\text{-}0\text{-}100\text{-}90}$ (309 kN.mm).

The beams of group II showed that the plate's spacing has a significant impact on the obtained values of absorbed energy. The absorbed energy of beams $B_{3\text{-}56\text{-}0\text{-}90}$, having contiguous plates, decreased by about 31% in comparison with beam $B_{3\text{-}56\text{-}100\text{-}90}$. Also, the recorded energy was decreased with the increase of plate's spacing. For instance, E was higher for beam $B_{3\text{-}56\text{-}150\text{-}90}$ (717 kN.mm) than that for beam $B_{3\text{-}56\text{-}200\text{-}90}$ (527 kN.mm). On the other hand, the plate's number slightly affected the recorded values of E. For beams $B_{4\text{-}56\text{-}100\text{-}90}$ and $B_{5\text{-}56\text{-}100\text{-}90}$ the values of E were about 860 and 852 kN.mm, respectively. That can be expected, as explained before, the plate's number slightly affected the ultimate capacity and deflection.

Regarding group IV, the decrease in plate's inclination angle slightly increased the value of E compared with the beam strengthened using vertical plates. The values of E for beams $B_{3\text{-}56\text{-}100\text{-}45}$ and $B_{3\text{-}56\text{-}100\text{-}60}$ were about 943 and 890 kN.mm, respectively, which were higher than that obtained by $B_{3\text{-}56\text{-}100\text{-}90}$. The increase in absorbed energy is attributed to the increases in beams capacities as well as the corresponding deflections developed when inclined plates were used.

3.6. Cracking evolution

3.6.1. Developed flexural cracks

Columns 3 and 4 of Table 5 summarize the flexural cracking measurements including the first flexural cracking load and the maximum flexural crack width near failure for all beams. For flexural cracks, the first crack occurred under the loading point at the section subjected to the maximum bending moment. As listed in Table 5, as expected, the flexural cracking loads are almost the same for all beams. The first flexural cracking load was around 42 and 44 kN. However, the recorded flexural crack width near failure was dependent on the sustained load near failure. For instance, the reference control beam, BC, exhibited the lowest flexural crack width near failure; the value of P_u was about 85 kN and the corresponding crack width was about 0.10 mm. On the other hand, beam $B_{3\text{-}56\text{-}100\text{-}45}$ showed the highest value of the flexural crack width near failure; the value of P_u was about 192.22 kN and the corresponding crack width was about 0.21 mm.

Table 5
Summary of first crack load and crack width at ultimate stage.

Group No.	Beam ID	Flexural cracks		Concrete shear cracks		PCBCPs shear cracks	
		P_{cr}, kN	W_{max}, mm	P_{cr}, kN	W_{max}, mm	P_{cr}, kN	W_{max}, mm
Control	BC	42	0.10	70	0.80	—	—
Group I	$B_{3\text{-}0\text{-}100\text{-}90}$	44	0.12	81	0.51	102	0.12
	$B_{3\text{-}28\text{-}100\text{-}90}$	43	0.14	82	0.53	103	0.11
	$B_{3\text{-}56\text{-}100\text{-}90}$	44	0.17	82	0.52	105	0.10
	$B_{3\text{-}84\text{-}100\text{-}90}$	44	0.20	81	0.55	105	0.10
Group II	$B_{3\text{-}56\text{-}0\text{-}90}$	43	0.15	90	0.61	103	0.06
	$B_{3\text{-}56\text{-}150\text{-}90}$	44	0.16	82	0.51	104	0.10
	$B_{3\text{-}56\text{-}200\text{-}90}$	42	0.13	81	0.52	104	0.11
Group III	$B_{4\text{-}56\text{-}100\text{-}90}$	43	0.18	80	0.50	106	0.10
	$B_{5\text{-}56\text{-}100\text{-}90}$	44	0.17	81	0.55	104	0.11
Group IV	$B_{3\text{-}56\text{-}100\text{-}45}$	44	0.21	82	0.55	107	0.09
	$B_{3\text{-}56\text{-}100\text{-}60}$	43	0.19	81	0.54	106	0.10

P_{cr} = first cracking load and W_{max} = relevant maximum crack width

3.6.2. Developed shear cracks on concrete substrate

Regarding the developed shear cracks on the concrete substrate, columns 5 and 6 of Table 5 list the shear cracking loads and the maximum shear crack widths near failure for all beams. As shown in Table 5, the first shear crack occurred in beam BC when the acting load reached about 70 kN. On the other hand, the concrete shear crack loads were affected by the used strengthening technique. The recorded concrete shear crack loads for the strengthened beams ranged between 80 and 90 kN. These increases may be attributed to the crack-arresting action of the used PCBCPs which altered the cracking pattern compared to that exhibited by beam BC.

With regard to the development of the shear crack widths in concrete, Figs. 14 to 17 show the load–major shear crack width curves for all tested beams. For group I, as shown in Fig. 14, attainment the cracking capacity of the control beam BC, the major shear crack width increased swiftly and reached about 0.8 mm in width near failure. Whereas, the application of PCBCPs, not only decreased the concrete major shear crack width corresponding to all load levels but also, prevented the rapid growth of concrete shear cracks. The fiber bridging phenomenon of the SHCC material delays the formation of cracks and limits the crack width growth. Moreover, the beams strengthened using reinforced PCBCPs,

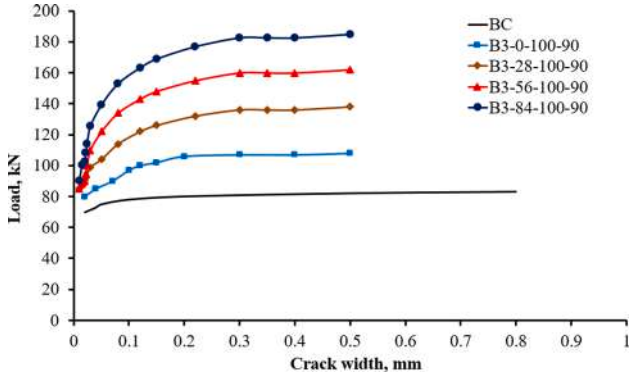


Fig. 14. load-crack width curves for all beams of group I.

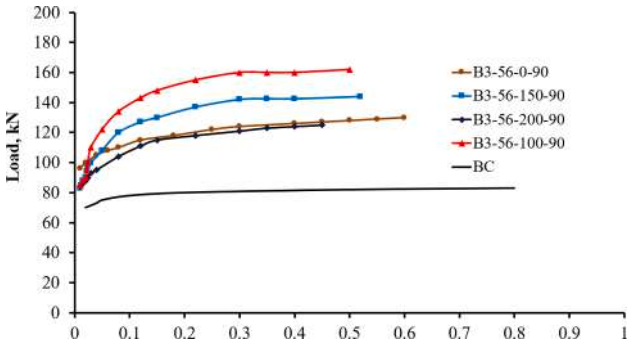


Fig. 15. load-crack width curves for all beams of group II.

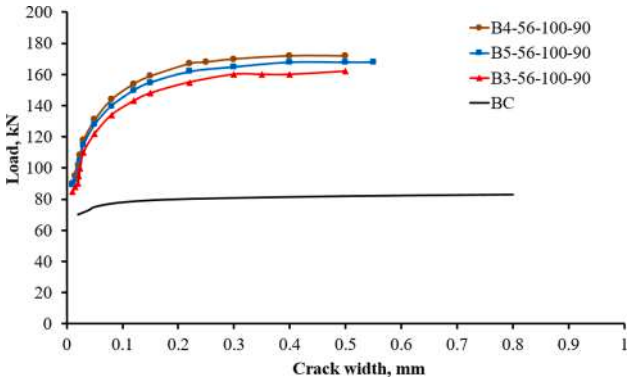


Fig. 16. load-crack width curves for all beams of group III.

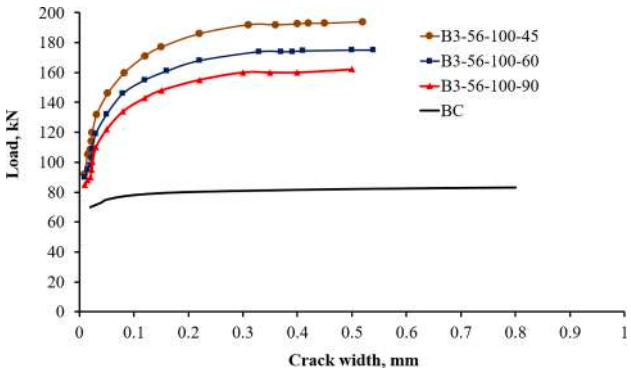


Fig. 17. load-crack width curves for all beams of group IV.

recorded narrower crack widths than that exhibited by beam $B_{3\text{-}0\text{-}100\text{-}90}$. For instance, for beam $B_{3\text{-}0\text{-}100\text{-}90}$, the major crack width was about 0.12 mm at load level of about 100 kN, whereas, at the same loading level, the recorded crack widths were about 0.04, 0.025, 0.015 mm for beams $B_{3\text{-}28\text{-}100\text{-}90}$, $B_{3\text{-}56\text{-}100\text{-}90}$ and $B_{3\text{-}84\text{-}100\text{-}90}$, respectively. This may be explained by; the use steel plates in conjunction with SHCC increased the axial stiffness of the PCBCPs, which controlled the cracks propagation.

Group II was designed to study the effect of plate's spacing, three different plate's spacing were studied; 0, 150, 200 mm. As shown in Fig. 15, while the plate's spacing was increased, the crack arresting action of the PCBCPs was decreased. Thus, the recorded crack widths for beams $B_{3\text{-}56\text{-}150\text{-}90}$ and $B_{3\text{-}56\text{-}200\text{-}90}$ were even wider than that recorded for beam $B_{3\text{-}56\text{-}100\text{-}90}$. For beam $B_{3\text{-}56\text{-}0\text{-}90}$, the use of contiguous plates delayed the crack occurrence, but once the shear cracks occurred in the un-strengthened part, the shear crack width rabidly increased to record a higher value than that developed by beam $B_{3\text{-}56\text{-}100\text{-}90}$.

As shown in Fig. 16, the increase of plate's number with a constant

clear spacing seems to be ineffective in limiting the shear crack width. Beams $B_{3\text{-}56\text{-}100\text{-}90}$, $B_{4\text{-}56\text{-}100\text{-}90}$ and $B_{5\text{-}56\text{-}100\text{-}90}$ showed almost a similar load-crack width response. The load-crack width curve of group IV is depicted in Fig. 17. It can be noticed that, the use of inclined PCBCPs controlled the crack widths compared to those recorded for beam having vertical PCBCPs. This may be attributed to that when the plate's inclination angle was near to the direction of principle stresses, the effectiveness of the used plates increased.

3.6.3. Developed shear cracks on PCBCPs

Columns 7 and 8 of Table 5 list the PCBCPs shear cracking loads and the maximum shear crack widths developed on the PCBCPs near failure for all strengthened beams. It can be observed that for all strengthened beams, cracks were developed on the PCBCPs after their preparation in the concrete substrate. For instance, for beam $B_{3\text{-}56\text{-}100\text{-}90}$, the first shear crack occurred in the PCBCPs when the acting load reached about 105 kN whereas cracks initiated on the adjacent concrete substrate at a vertical load of about 82 kN. This difference is attributed to the enhanced tensile characteristics of the SHCC material in comparison with the ordinary concrete. Moreover, contrary to the ordinary concrete, the fibers crossing the crack surfaces in the SHCC can restrict the crack widening, leading to multiple cracks generation. Thus, for the same beam, near failure the shear crack width in the PCBCPs was lower than that developed in concrete substrate. For instance, for beam $B_{3\text{-}56\text{-}100\text{-}90}$, near failure, the recorded shear crack width in the PCBCPs was about 0.10 mm, while the recorded one the adjacent concrete substrate was about 0.52 mm.

3.7. Estimation of maximum shear crack width on RC beams

Previous studies have documented that the developed maximum shear crack width in RC beams is mainly dependent on several parameters such as the web reinforcement ratio [41,42], the developed tensile strain in the web reinforcement [41,43], the concrete compressive strength [44], the size effect [45,46], the developed normal strain on the longitudinal steel reinforcing bars [47,48], the side concrete cover at the shear span zone [47], the amount and distribution of the web reinforcement [48], the bond characteristics of the web reinforcement [49], the angle with member axis and shear span-to-depth ratio [49]. Over years, researchers have devoted their effort to develop an accurate model to estimate the maximum shear crack width in RC beams [43,44,49–52]. However, it was found that the proposed equation by Zakaria et al. [52] is the most general equation since it included many affecting parameters on the shear crack width. Therefore, this equation was adopted in the current study in order to verify its applicability on estimating the shear crack width for the strengthened beams.

Zakaria et al. [52] assumed Eq. (5) for estimating the average shear crack width (w_{av})based on regression analysis.

$$w_{av} = 0.112 k_s k_t (c_s)^{0.05} \left(\frac{1}{\rho_w}\right)^{0.207} \left(\frac{1}{\rho_l}\right)^{0.252} (1.25 s_{m\theta}) \varepsilon_w \quad (5)$$

Wherek_s = coefficient taking into account the shear reinforcement hook type = 1 for closed ordinary stirrups;k_t = coefficient taking into account the type of shear reinforcement = 1.2 for smooth plain bars;$c_s$is side concrete cover for shear reinforcement; ρ_w is the web reinforcement ratio = $\frac{A_w}{b_w s_y}$; A_w = the total cross-sectional area of vertical legs of stirrups in one row that can be calculated by Eqs. (6) and (7) for the case of PCBCPs;b_w = the width of the beam; s_y = horizontal spacing between vertical stirrups; ρ_l is the longitudinal reinforcement ratio;$s_{m\theta}$ = the average spacing of shear cracks that can be calculated by Eqs. (8), (9) and (10);ε_w is the stirrup strain.

$$A_w = A_{sp} + A_{SHCC} \frac{E_{SHCC}}{E_s} \quad (6)$$

Where A_{sp} = cross-sectional area of internal steel plate; A_{SHCC} = cross-sectional area of the precast SHCC plate; E_s = modulus of elasticity of steel forming steel plates; E_{SHCC}= modulus of elasticity of SHCC material as given in Eq. (7) according to JSCE [28].

$$E_{SHCC} = 1.77 * 10^4 \sqrt{\frac{\gamma}{18.5}} \left(\frac{f_{ck}}{60}\right)^{\frac{1}{3}} \quad (7)$$

γ = coefficient = 23;f_{ck} = concrete compressive cylinder strength.

$$s_{m\theta} = \left[\frac{1}{\frac{\sin\theta}{s_{mx}} + \frac{\cos\theta}{s_{my}}}\right] \quad (8)$$

Where θ = the inclination angle of the major shear crack with horizontal axis; s_{mx} and s_{my} are the horizontal and vertical crack spacing, respectively, as given by Eqs. (9) and (10).

$$s_{mx} = 2\alpha_1 \left[c_x + \frac{s_x}{10}\right] + k_1 k_2 \alpha_1 \frac{d_{bx}}{\rho_x} \quad (9)$$

$$s_{my} = 2\beta_1 \left[c_y + \frac{s_y}{10}\right] + k_1 k_2 \beta_1 \frac{d_{bv}}{\rho_v} \quad (10)$$

Where c_x is the distance from the horizontal center line of the concrete cross-section to longitudinal reinforcements; c_y is the distance from the center line of the concrete cross-section to the inner edge of vertical reinforcement; s_x is the spacing between longitudinal reinforcement; s_y is the spacing between web reinforcement; k_1 is the bond coefficient = 0.8 for smooth bars; k_2 is the stress distribution coefficient; d_{bx} is the diameter of longitudinal bars; d_{bv} is the diameter of web reinforcement; ρ_x is the longitudinal reinforcement ratio; ρ_v is the web reinforcement ratio; α_1 and β_1 are correlation factors equal to 0.36.

It is worth mentioning that the available equations for calculating the average shear crack width such as Eq. (5) did not state the load level corresponding to the estimated shear crack width, i.e., the proposed shear crack width is corresponding to the failure load of the beam or at a specific level of the acting load. Besides, this equation was proposed for RC beams reinforced with internal stirrups. Inspite that Eq. (5) was used for calculating the average shear crack width for the current study pertaining to RC beams without internal stirrups and reinforced with PCBCPs. That is to verify the applicability of the adopted equation on the current strengthened beams incorporating some modifications to replace the PCBCPs by equivalent steel stirrups.

Table 6 compares the results of the experimental maximum shear crack widths against the estimated ones based on the adopted model (Eq. (5)). It can be observed that the adopted model showed conservative results for all strengthened beams, where the measured shear crack widths represented more than three times of the estimated ones. However, the measured shear crack widths for all strengthened beams were noticed to be increased proportionate to the applied load till a maximum shear crack width of about 0.3 mm, and then the shear crack widths were increased swiftly without increased loading as depicted in Figs. 14 to 17. Therefore, the maximum shear crack width was assumed to be 0.3 mm for all strengthened beam and compared with the estimated shear crack widths. Once more, the adopted model showed conservative results. Thus, it can be concluded that the adopted model by Zakaria et al. [52] can be applied properly for estimating the average shear crack widths for the strengthened beams of the current study.

As illustrated in the previous section that the propagated shear cracks in the PCBCPs were narrower than that developed in the concrete substrate. Thus, another comparison was made for the maximum shear crack widths developed on the PCBCPs. As illustrated in Table 6, the adopted model exhibited higher shear crack widths than those developed on the PCBCPs where the developed shear crack widths on the PCBCPs represented 0.59 to 0.73 of the corresponding estimated ones that were about 0.64 on an average sense exclusive the results of beam reinforced with contiguous plates ($B_{3\text{-}56\text{-}0\text{-}90}$). In sum, the adopted model

Table 6
Comparison between the experimental shear crack widths against estimated ones.

Group No.	Beam ID	$W_{max(concrete)}$, mm	$W_{max(PCBCP)}$, mm	$W_{analytical}$, mm [52]	$W_{max(concrete)}/W_{analytical}$	$0.3/W_{analytical}$	$W_{max(PCBCP)}/W_{analytical}$
Control	BC	0.80	—	—	—	—	—
Group I	$B_{3\text{-}0\text{-}100\text{-}90}$	0.51	0.12	0.165	3.09	1.82	0.73
	$B_{3\text{-}28\text{-}100\text{-}90}$	0.53	0.11	0.158	3.36	1.90	0.70
	$B_{3\text{-}56\text{-}100\text{-}90}$	0.52	0.10	0.151	3.44	1.98	0.66
	$B_{3\text{-}84\text{-}100\text{-}90}$	0.55	0.10	0.146	3.77	2.06	0.69
Group II	$B_{3\text{-}56\text{-}0\text{-}90}$	0.61	0.06	0.294	2.07	1.02	0.20
	$B_{3\text{-}56\text{-}150\text{-}90}$	0.51	0.10	0.170	3.00	1.77	0.59
	$B_{3\text{-}56\text{-}200\text{-}90}$	0.52	0.11	0.186	2.80	1.61	0.59
Group III	$B_{4\text{-}56\text{-}100\text{-}90}$	0.50	0.10	0.151	3.31	1.98	0.66
	$B_{5\text{-}56\text{-}100\text{-}90}$	0.55	0.11	0.151	3.64	1.98	0.73
Group IV	$B_{3\text{-}56\text{-}100\text{-}45}$	0.55	0.09	0.153	3.60	1.96	0.59
	$B_{3\text{-}56\text{-}100\text{-}60}$	0.54	0.10	0.152	3.55	1.97	0.66

by Zakaria et al. [52] can be used rationally to estimate the average shear crack width developed on RC strengthened beams by PCBCPs. Besides, the estimated shear crack width represents at least 0.59 of the developed shear crack width on the PCBCPs. However, an accurate model have to be developed for estimating the major shear cracks widths on both the concrete substrate and the PCBCPs taking into account the controlling parameters for such strengthening technique.

3.8. Developed normal strain on internal steel plates

The developed normal strains on the used steel plates inside the PCBCPs were recorded using electrical strain gauges bonded at the mid height of each steel plate, as presented in Fig. 5(a). Figs. 18 to 21 show the applied vertical load versus steel plates strain relationships for all tested beams. Generally, it can be observed that, at the same loading level, the outer steel plates exhibited lower strains compared to that of the intermediate plate. This is expected, as the major shear cracks passed through the middle part of the shear span zone. Also, near failure, the middle plate recorded the highest strain value in comparison with those placed at the edges of the shear span zone. For instance, for beam $B_{3\text{-}56\text{-}100\text{-}90}$, the strain recorded in middle plate near failure was about 2300 με vs. 1388 and 1460 με for the outer plates. As shown in Figs. 18 to 21, excluding beam $B_{3\text{-}56\text{-}0\text{-}90}$ with contiguous PCBCPs, at least one of the internal steel plates reached the yield strain (yield strain = 1213 με). On the other hand, for $B_{3\text{-}56\text{-}0\text{-}90}$, the maximum strain developed on the middle steel plate of was about 145 με. This observation is consistent with the obtained cracking pattern of $B_{3\text{-}56\text{-}0\text{-}90}$, as shown in Fig. 8, the shear cracks did not intersect with the PCBCPs.

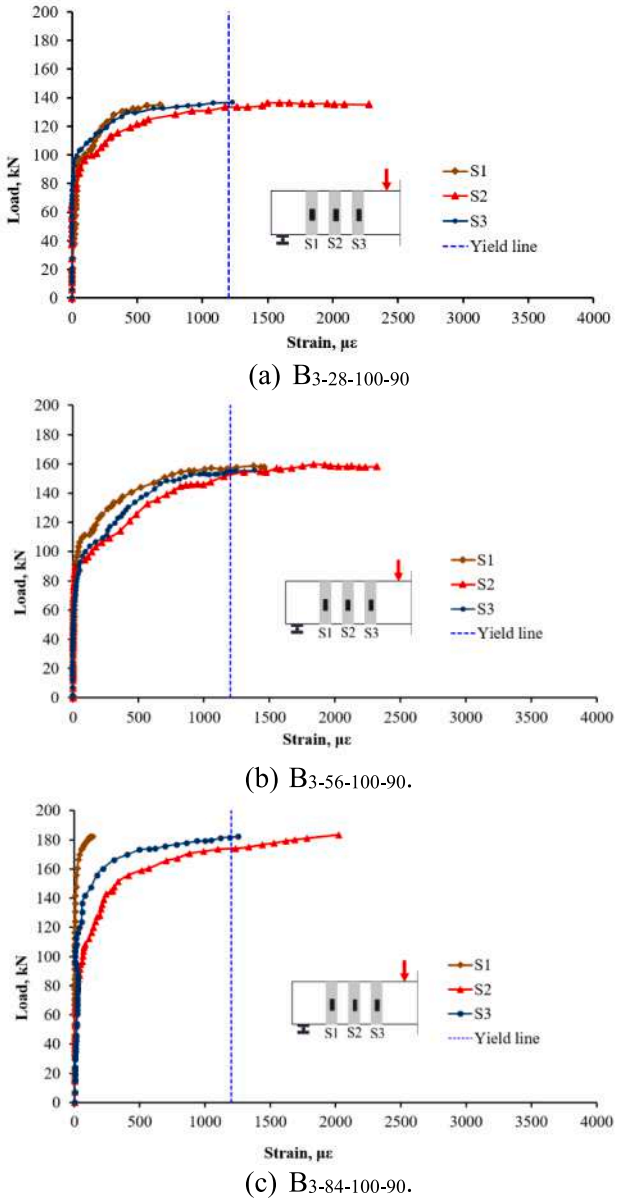
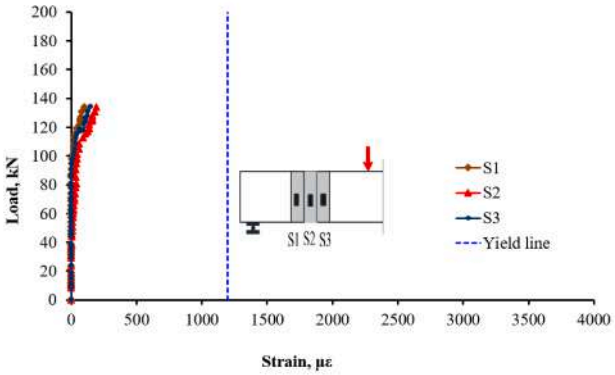


Fig. 18. Load-developed normal strain curves on steel plates inside PCBCPs for all beams of group I.

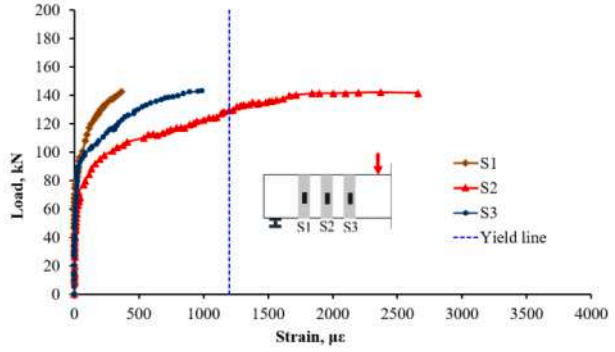
4. Conclusion

Based on the results of the experimental tests pertaining to the used concrete dimensions and reinforcement detailing accompanied with the loading protocol considering the studied parameters of the used precast cement-based composite plates (PCBCPs), the following conclusions could be drawn:

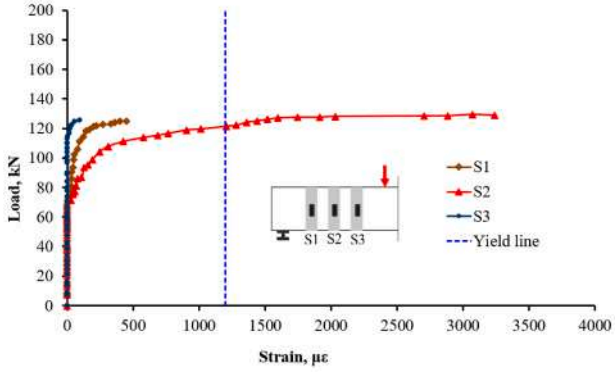
1. The adopted strengthening technique for shear-deficient RC beams based on precast cement-based composite plates (PCBCPs) showed its efficiency in enhancing the ultimate shear capacity of the strengthened beams even that the used PCBCPs were made of plain SHCC. The beam strengthened with plain PCBCPs showed about 29% increases in its shear capacity compared to that of the control un-strengthened beam. Providing internal thin steel plate inside the PCBCPs enabled the strengthened beam to develop higher shear capacity, which was directly proportionate to the used amount of the internal steel plate. The gain in the ultimate capacity can reach up to about 115% when the reinforcement ratio of internal steel plate was 4.25%.
2. Increasing the clear spacing between the used PCBCPs resulted in declined the gain of the ultimate capacity. Hence, the best performance for the strengthened beams was obtained when the clear spacing between the used PCBCPs was 100 mm. That allowed more than one plate to intersect with the developed major shear



(a) $B_{3\text{-}56\text{-}0\text{-}90}$



(b) $B_{3\text{-}56\text{-}150\text{-}90}$

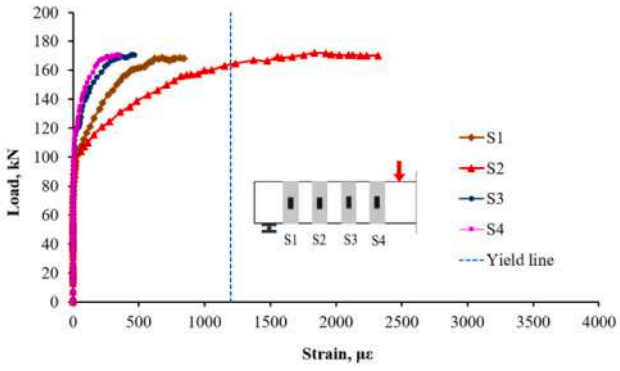


(c) $B_{3\text{-}56\text{-}200\text{-}90}$

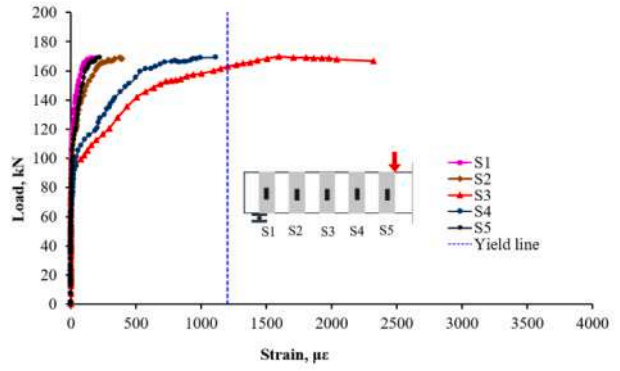
Fig. 19. Load-developed normal strain curves on steel plates inside PCBCPs for all beams of group II.

crack, thus restrict its propagation. As a result, the shear capacity could be enhanced effectively.

3. Using inclined PCBCPs has better effect than that provided by vertical PCBCPs, especially when the plates were positioned to be perpendicular to the line connecting the load and reaction points. The shear capacity of $B_{3\text{-}56\text{-}100\text{-}45}$ (192.22 kN) and $B_{3\text{-}56\text{-}100\text{-}60}$ (175.17kN) were about 20% and 9% higher than that of $B_{3\text{-}56\text{-}100\text{-}90}$ (160.50 kN) having identical vertical plates, respectively.
4. The application of PCBCPs hindered the appearance of shear cracks on the substrate beam. That could be attributed to the crack-arresting action of the used PCBCPs which altered the cracking pattern compared to that exhibited by the control beam BC.
5. The developed major shear crack width is sensitive to the percentage of internal steel plate ratio, the clear spacing and the inclination angle of the used PCBCPs.
6. The best performance for the strengthened beams from both strength gain and the limiting of the major shear crack width was obtained when inclined PCBCPs by 45° was used.

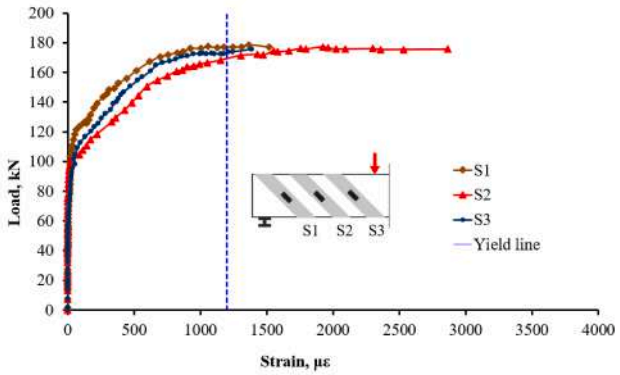


(a) $B_{4\text{-}56\text{-}100\text{-}90}$

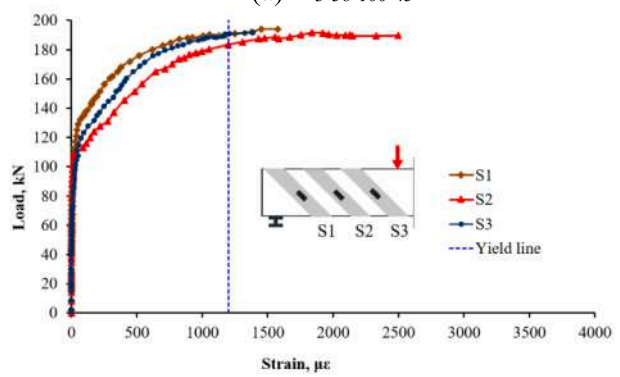


(a) $B_{5\text{-}56\text{-}100\text{-}90}$

Fig. 20. Load-developed normal strain curves on steel plates inside PCBCPs for all beams of group III.



(a) $B_{3\text{-}56\text{-}100\text{-}45}$



(a) $B_{3\text{-}56\text{-}100\text{-}60}$

Fig. 21. Load-developed normal strain curves on steel plates inside PCBCPs for all beams of group IV.

7. The available models for the ultimate shear capacity and the average shear crack width can be applied rationally for the strengthened beams by PCBCPs.

5. Data availability

The raw data required to reproduce these findings are available only with direct contact through email to the corresponding author. The processed data required to reproduce these findings are available only with direct contact through email to the corresponding author.

Declaration of Competing Interest

The authors declare that they have no known competing financial interests or personal relationships that could have appeared to influence the work reported in this paper.

References

[1] Adhikary BB, Mutsuyoshi H, Sano M. Shear strengthening of reinforced concrete beams using steel plates bonded on beam web: experiments and analysis. Constr Build Mater 2000;14(5):237–44.
[2] Barnes RA, Baglin PS, Mays GC, Subedi NK. External steel plate systems for the shear strengthening of reinforced concrete beams. Eng Struct 2011;23(9):1162–76.
[3] Adhikary BB, Mutsuyoshi H. Shear strengthening of RC beams with web bonded continuous steel plates. Constr Build Mater 2006;20(5):296–307.
[4] Adhikary BB, Mutsuyoshi H. Shear strengthening of reinforced concrete beams using various techniques. Constr Build Mater 2006;20(6):366–73.
[5] Barnes RA, Mays GC. Strengthening of reinforced concrete beams in shear by the use of externally bonded steel plates: Part 1–Experimental program. Constr Build Mater 2006;20(6):396–402.
[6] Altin S, Anil Ö, Kara ME. Improving shear capacity of existing RC beams using external bonding of steel plates. Eng Struct 2005;27(5):781–91.
[7] Afefy HM, Fawzy TM. Strengthening of RC one-way slabs including cut-out using different techniques. Eng Struct 2013;57:23–36.
[8] Afefy HM, Kassem NM, Mahmoud MH. Retrofitting of faulty reinforced concrete frame structures using two strengthening techniques. Mag Concr Res 2016;71(6):309–24.
[9] Afefy HM, Baraghith AT, Mahmoud MH. Retrofitting of defected RC cantilever slabs using different techniques. Mag Concr Res 2020;72(14):703–19.
[10] Li VC. From micromechanics to structural engineering-the design of cementitious composites for civil engineering applications. JSCE J Struct Mech Eq Eng 1993; 10 (2):3748.
[11] Li VC, Kanda T. Engineered cementitious composites for structural applications. J Mater Civ Eng 1998;10(2):66–79.
[12] Li VC, Wang S, Wu C. Tensile strain-hardening behavior of polyvinyl alcohol engineered cementitious composite (PVA-ECC). ACI Mater J 2001;98(6):483–92.
[13] Li VC, Wang S, Ogawa A, Saito T. Interface tailoring for strain-hardening PVA-ECC. ACI Mater J 2002;99(5):463–72.
[14] Li VC. Engineered cementitious composites (ECC) - a review of the material and its applications. J Adv Concr Tech 2003;1(3):215–30.
[15] Afefy HM, Kassem NM, Hussein M. Enhancement of flexural behavior of CFRP strengthened reinforced concrete beams using engineered cementitious composites transition layer. Struct Infrastruct Eng 2015;11(8):1042–53.
[16] Yu J, Leung CKY. Strength improvement of strain-hardening cementitious composites with ultra highvolume fly ash. J Mater Civ Eng 2017;29:05017003.
[17] Kassem M, El-Shafeiy T, Hussein M, Afefy HM, Hassan A. Shear behaviour of SHCC dry joints in precast construction. International Conference on Advances in Structural and Geotechnical Engineering, ICASGE'17, Hurghada, Egypt, 27-30 March 2017.
[18] Baghi H, Barros JAO, Rezazadeh M. Shear strengthening of damaged reinforced concrete beams with Hybrid Composite Plates. Compos Struct 2017;178:353–71.
[19] Li J, Weng J, Yang E. Stochastic model of tensile behavior of strain-hardening cementitious composites (SHCCs). Cem Concr Res 2019;124:105856.
[20] Wang G, Yang C, Pan Y, Zhu F, Jin K, Li K, et al. Shear behaviors of RC beams externally strengthened with engineered cementitious composite layers. Mater 2019;12:2163.
[21] Elnagar AB, Afefy HM, Baraghith AT, Mahmoud MH. Experimental and numerical investigations on the impact resistance of SHCC-strengthened RC slabs subjected to drop weight loading. Constr Build Mater 2019;229:116866.
[22] Afefy HM, Kassem NM, Taher SF. Retrofitting of defected closure strips for full-depth precast concrete deck slabs using EB-CFRP sheets. Pract Period Struct Des Constr 2019;24(4):04019025.
[23] Zheng YZ, Wang WW, Mosalam KM, Fang Q, Chen L, Zhu ZF. Experimental investigation and numerical analysis of RC beams shear strengthened with FRP/ECC composite layer. Compos Struct 2020;246:112436.
[24] Yang X, Gao WY, Dai JG, Lu ZD. Shear strengthening of RC beams with FRP grid-reinforced ECC matrix. Compos Struct 2020;241:112120.
[25] Shang Xy Yu, Jt LL, Lu Zd. Shear strengthening of fire damaged RC beams with stirrup reinforced engineered cementitious composites. Eng Struct 2020;210:110263.
[26] Hassan A, Atta AM, El-Shafiey TF. Restoration of the shear capacity for RC beams with web openings using precast SHCC plates. Struct 2020;25:603–12.
[27] Li VC, Li M. Durability performance of ductile concrete structures. Proceedings of the 8th international conference on creep, shrinkage and durability of concrete and concrete structures, Ise-Shima, Japan. 2008. p. 761-8.
[28] Japan Society of Civil Engineers. Recommendations for design and construction of high performance fiber reinforced cement composite with multiple fine cracks (HPFRCC), Concrete engineering series 82, 2008.
[29] Kunieda M, Rokugo K. Recent progress of HPFRCC in Japan - Required performance and applications. J Adv Concr Technol 2006;4(1):19–33.
[30] Kunieda M, Denarie E, Bruhwiler E, Nakamura H. Challenges for strain hardening cementitious composites -Deformability versus matrix 2007.
[31] Fischer G, Li V. Influence of matrix ductility on tension-stiffening behavior of steel reinforced engineered cementitious composites (ECC). ACI Struct J 2002;99(1):104–11.
[32] Rokugo K, Lim SC, Kanda T, Kunieda M, Fujimoto Y. Tensile behavior of ECC members with or without reinforcement. In: Proc. of International RILEM Workshop on HPFRCC in Structural Applications; 2005. p. 279–86.
[33] Kunieda M, Hussein M, Ueda N, Nakamura H. Enhancement of crack distribution of UHP-SHCC under axial tension using steel reinforcement. J Adv Concr Technol 2010;8:49–57.
[34] ACI Committee 318 (2019). Building Code Requirements for Structural Concrete (ACI 318-19) and Commentary (ACI 318R-19). American Concrete Institute, Farmington Hills, MI, 519 ppfv.
[35] ASTM C39/C39M-20, Standard Test Method for Compressive Strength of Cylindrical Concrete Specimens, ASTM International, West Conshohocken, PA, 2020, www.astm.org.
[36] ASTM A770/A770M-03(2018), Standard Specification for Through-Thickness Tension Testing of Steel Plates for Special Applications, ASTM International, West Conshohocken, PA, 2018, www.astm.org.
[37] Egyptian code for design and construction of reinforced concrete structures (ECP 203–2019); 2019.
[38] Gendron G, Picard A, Guerin M. A theoretical study on shear strengthening of reinforced concrete beams using composite plates. Compos Struct 1999;45:303–9.
[39] Ding Z, Xu MR, Dai JG, Dong BQ, Zhang MJ, Hong SX, et al. Strengthening concrete using phosphate cement-based fiber-reinforced inorganic composites for improved fire resistance. Constr Build Mater 2019;212:755–64.
[40] Jiang CJ, Lu ZD, Li LZ. Shear performance of fire-damaged reinforced concrete beams repaired by a bolted side-plating technique. J Struct Eng 2017;143(5):04017007.
[41] Witchukreangkrai E, Mutsuyoshi H, Takagi M, De Silva S. Evaluation of shear crack width in partially prestressed concrete members. Proceedings JCI 2006;28(2):823–8.
[42] Rizkalla SH, Hwang LS, El Shahawai M. Transverse reinforcement effect on cracking behavior of RC members. Canadian J Civ Eng 1983;10(4):566–81.
[43] De Silva S, Mutsuyoshi H, Witchukreangkrai E. Evaluation of shear crack width in I-shaped prestressed reinforced concrete beams. J Adv Concr Technol 2008;6(3):443–58.
[44] Piyamahant S. Shear behavior of reinforced concrete beams with a small amount of web reinforcement. M. Eng. Dissertation. Japan: Kochi University of Technology; 2002.
[45] Shioya T, Iguro M, Nojiri Y, Akiyama H, Okada T. Shear strength of large reinforced concrete beams. Fracture Mechanics: Application to Concrete, SP 118, American Concrete Institute, Detroit, 309. 1989.
[46] Sherwood EG, Bentz EC, Collins MP. Effect of aggregate size on beam-shear strength of thick slabs. ACI Struct J 2007;104(2):180–90.
[47] Adebar P, Leeuwen JV. Side-face reinforcement for flexural and diagonal cracking in large concrete beams. ACI Struct J 1999;96(5):693–704.
[48] Zararis PD. Shear strength and minimum shear reinforcement of RC slender beams. ACI Struct J 2003;100:203–14.
[49] Hassan HM. Shear cracking behavior and shear resisting mechanism of reinforced concrete beams with web reinforcement. PhD. Thesis. Japan: University of Tokyo; 1987.
[50] Fukuyama H, Suwada H, Iso M, Matsuzaki Y, Nakano K, Kasahara M. Evaluation of damage limit state of RC element due to shear crack width. Proceedings of Architectural Institute of Japan (AIJ), (C-2) 2000, 13-14. (in Japanese).
[51] Witchukreangkrai E, Mutsuyoshi H, Takagi M, De Silva S. Evalustion of shear crack width in partially pre-stressed concrete members. Proceedings JCI 2006; 28(2):823-828.
[52] Zakaria M, Ueda T, WE Z. Evaluating and proposing prediction models for shear crack width in concrete beams. J Japan Society Civil Eng, (Mater Concr Struct) 2011;67(2):245–63.